Frontiers of Information Technology & Electronic Engineering
www.jzus.zju.edu.cn; engineering.cae.cn; www.springerlink.com
ISSN 2095-9184 (print); ISSN 2095-9230 (online)
E-mail: jzus@zju.edu.cn

Broadband and asymmetrical Doherty based on circuit parameter solution space*

Cheng BI[1], Haotian LI[2], Shuai WANG[2], Zhijiang DAI[†‡1], Jingzhou PANG[1], Ruibin GAO[1], Kang ZHONG[1], Jingsong WANG[1]

[1]*School of Microelectronics and Communication Engineering, Chongqing University, Chongqing 400044, China*

[2]*The 54th Research Institute of China Electronics Technology Group Corporation, Shijiazhuang 050081, China*

[†]E-mail: daizj_ok@126.com

Received Mar. 23, 2024; Revision accepted May 30, 2024; Crosschecked Sept. 26, 2024

Abstract: The input impedance of the post-matching network (PMN) is configured as a complex value. The parameter solution space is determined based on the fundamental principles of the Doherty power amplifier (DPA), enabling the DPA to achieve high efficiency at the output power back-off (OBO). The parameter solution space comprises three variables: the phase parameter of the output matching network for the carrier power amplifier (carrier PA), the phase parameter of the output matching network for the peaking power amplifier (peaking PA), and the input impedance of PMN. These parameters are optimized to enable the DPA to achieve high efficiency at the OBO. In this paper, a one-to-one mapping relationship is established between the frequency and the parameter solution space, allowing for a precise optimization of the DPA across a broad frequency range. Leveraging this mapping relationship, an asymmetric DPA designed to operate over the 1.8–2.6 GHz frequency band is designed and fabricated, demonstrating the feasibility and effectiveness of the proposed approach. Under continuous wave excitation, the test results show that the drain efficiency (DE) is 42.7%–56.4% at 9.5 dB OBO and the saturated DE is 45.8%–71.1%. The saturated output power of this DPA is 46.9–48.8 dBm with a gain of 5.5–8.0 dB at saturation. A 20-MHz long-term-evolution modulated signal with a peak-to-average power ratio of 8 dB is also applied to the fabricated DPA at 1.8, 2.1, and 2.6 GHz. Under these conditions, at 8 dB OBO, the DPA shows an adjacent channel power ratio always lower than 48 dBc after digital pre-distortion linearization.

Key words: Doherty power amplifier; Output matching network; Parameter solution space
https://doi.org/10.1631/FITEE.2400226 **CLC number:** TN722

1 Introduction

Power amplifier (PA) is one of the key components of the mobile communication system and the radar system. It plays a pivotal role in the functioning of the whole system (Li M et al., 2022). Stepping into the fifth generation (5G) wireless network era, the architecture of large-scale multiple-input multiple-output (MIMO) transmitters is the focus of the current research. Therefore, with the increase of the number of frequency bands to be covered by the transmitter, it is imperative to broaden the bandwidth of the radio frequency (RF) amplifier (Cavarroc et al., 2023). To improve the spectrum efficiency, the modulated signal with a high peak-to-average power ratio (PAPR) is usually used, which requires the amplifier to provide efficient performance not only at saturation but also at output power back-off (OBO) (Xu et al., 2021). Therefore, PA that can achieve high efficiency at the OBO is an excellent

‡ Corresponding author

* Project supported by the National Key Laboratory of Science and Technology on Space Microwave, China (No. HTKJ2023KL504005) and the Funds in the Field of Technology of the Enhanced Program of National Basic Research, China (No. 2022-JCJQ-JJ-0637)

ORCID: Cheng BI, https://orcid.org/0009-0009-7061-0924; Zhijiang DAI, https://orcid.org/0000-0003-4914-1464

choice for the industry. In the past few decades, many technologies and architectures have been proposed to achieve high efficiency at the OBO, such as Doherty power amplifier (DPA) (Doherty, 1936), load modulated balanced amplifier (LMBA) (Chen et al., 2023), and outphasing (Li SS et al., 2021). Among them, DPA has become one of the most popular technologies because of its simple circuit structure and high reliability. The traditional DPA that uses the same type of transistors in the main circuit and auxiliary circuit can achieve high efficiency at 6 dB OBO, but the broadband performance of the traditional DPA is not very good (Zhang JR et al., 2023). Therefore, designing DPAs with a certain bandwidth has become a research hotspot. Hallberg et al. (2016) treated the output matching network as a black box whose parameters (the impedance of the carrier PA at the current source plane and the combining impedance) and the input phase delay were solved according to the given transistor characteristics and design requirements. Based on this theory, a symmetric Doherty PA operating at 2.14 GHz was designed. Yang et al. (2019) designed a broadband PA operating at 1.1–2.4 GHz using the complex combining load (CCL) with noninfinity peaking impedance. Bachi et al. (2022) proposed a new combiner analysis method for the design of DPAs, based on which a class-E power amplifier operating at 1.1–2.4 GHz was designed in a 130 nm radio frequency silicon-on-insulator (RF-SOI) process.

Nowadays, the modulated signals in communication equipment tend to use the modulated signals with high PAPR, which requires the PA to achieve high efficiency at a higher OBO level (higher than 9 dB). The traditional DPA has an OBO of only 6 dB. Therefore, in recent years, many scholars have improved the Doherty architecture to achieve high efficiency at higher OBO, such as through three-way Doherty architecture (Zhang XH et al., 2023), asymmetric Doherty architecture (Rouhani et al., 2020; Li MY et al., 2023), and CCL impedance (Fang and Cheng, 2014). In the present study, different transistors are used in the main road and the auxiliary road. This asymmetric structure is used to expand the OBO level. Meanwhile, the input impedance of the post-matching network (PMN) is designed as a complex value, and then the solution space $[\theta_{\mathrm{C}}, \theta_{\mathrm{P}}, Z_{\mathrm{L}}]$ that makes the DPA achieve high efficiency at the OBO is solved. The one-to-one mapping relationship is set between the frequency and $[\theta_{\mathrm{C}}, \theta_{\mathrm{P}}, Z_{\mathrm{L}}]$ so that these three parameters vary linearly with frequency. Based on the mapping relationship, an asymmetric DPA working over 1.8–2.6 GHz is designed using GaN high-electron mobility transistor (HEMT) devices.

2 Theoretical analysis of the proposed Doherty power amplifier (DPA)

2.1 Expanding the output power back-off (OBO) level by using asymmetric cells

The simplified schematic of the traditional DPA is shown in Fig. 1. The DPA consists of two amplifiers: a class-B biased carrier PA (main) and a class-C biased peaking PA (auxiliary). Two current generators (I_{C} and I_{P}) represent the carrier PA and the peaking PA, respectively. The principle of the DPA is to increase the impedance at the current source plane (Z_{C} in Fig. 1) at the OBO level so that the voltage of the carrier PA can reach saturation, thus improving the efficiency. The $\mathrm{OMN_c}$ is the output matching network of the carrier PA. $\mathrm{OMN_p}$ is the output matching network of the peaking PA. PMN represents the post-matching network. If the carrier PA and the peaking PA use the same drain bias voltage, the OBO level of the DPA can be defined as in Eq. (1):

$$\mathrm{OBO} = 20\lg(1+\delta), \tag{1}$$

where δ is the ratio of I_{C1} to I_{P1} in the saturated state (Son et al., 2011; Pang et al., 2016), and I_{C1} and I_{P1} represent the current of the carrier PA and peaking PA at the combining point, respectively.

According to the traditional DPA theory, Z_{C}, Z_{P} (the impedance of the carrier PA and peaking PA at the current source plane, respectively), I_{C1}, I_{P1} (the impedance of the carrier PA and peaking PA at the combining point, respectively), and Z_{L} (the input impedance of the PMN) should satisfy the following relationship (Pang et al., 2016):

$$Z_{\mathrm{C}} = \begin{cases} (1+\delta)\, R_{\mathrm{opt\_c}}, & \mathrm{OBO}, \\ R_{\mathrm{opt\_c}}, & \mathrm{SAT}, \end{cases} \tag{2}$$

$$Z_{\mathrm{P}} = R_{\mathrm{opt\_p}}, \quad \mathrm{SAT}, \tag{3}$$

$$Z_{\mathrm{C1}} = \begin{cases} Z_{\mathrm{L}}, & \mathrm{OBO}, \\ (1+\delta)\, Z_{\mathrm{L}}, & \mathrm{SAT}, \end{cases} \tag{4}$$

$$Z_{\mathrm{P1}} = \left(1+\tfrac{1}{\delta}\right) Z_{\mathrm{L}}, \quad \mathrm{SAT}, \tag{5}$$

$$Z_{\mathrm{L}} = \frac{R_{\mathrm{opt\_c}}}{\delta+1}, \tag{6}$$

where SAT represents the saturation state at which the carrier PA and peaking PA reach saturation.

In this paper, the carrier PA uses the CGH40025F transistor of MACOM with a maximum drain output current of 3 A, and the peaking PA uses the CGH40045F transistor of MACOM with a maximum drain output current of 6 A. Therefore, δ, the current ratio of the two PAs in the saturated state, is set to 2. The drain biases are both set as 28 V. According to Eq. (1), the 9.5 dB OBO level can be achieved. $R_{\mathrm{opt\_c}}$ and $R_{\mathrm{opt\_p}}$ are 18.6 and 9.3 Ω, respectively, based on $R_{\mathrm{opt}} = 2V_{\mathrm{CC}}/I_{\max}$ (Yang et al., 2019). The impedance Z_{C}, Z_{P}, Z_{C1}, Z_{P1}, and Z_{L} can be calculated by Eqs. (2)–(6).

2.2 Solving the parameter solution space of DPA

The performance of DPA depends on its efficiency at OBO. Its efficiency at OBO is determined by Z_{CB} (which is the impedance Z_{C} at the OBO in Fig. 1). The impedance Z_{C} can be expressed in terms of the ABCD parameters as given by (Li M et al., 2019)

$$Z_{\mathrm{C}} = \frac{A_{\mathrm{C}} Z_{\mathrm{C1}} + B_{\mathrm{C}}}{C_{\mathrm{C}} Z_{\mathrm{C1}} + D_{\mathrm{C}}}. \tag{7}$$

Therefore, to calculate the impedance Z_{CB}, four parameters of the ABCD matrix of $\mathrm{OMN_c}$ and Z_{C1B} which is the impedance I_{C1} at the OBO are required to be calculated.

2.2.1 Solving the ABCD matrix of DPA

To obtain the ABCD matrix of $\mathrm{OMN_c}$, the scattering coefficient can be calculated first. According to Fig. 1, set the reference impedance of port 1 of $\mathrm{OMN_c}$ as $R_{\mathrm{opt\_c}}$, and set the reference impedance of port 2 as $(1+\delta)Z_{\mathrm{L}}$. When DPA works at saturation, port 1 and port 2 of $\mathrm{OMN_c}$ are connected with the matching impedance. According to the definition of the scattering coefficient, $S_{11} = S_{22} = 0$. Since $\mathrm{OMN_c}$ is lossless and reciprocal, the scattering coefficient matrix of $\mathrm{OMN_c}$ is shown in Eq. (8). The scattering coefficient of $\mathrm{OMN_p}$ can also be analyzed according to the same principle. Set the reference impedance of port 1 of $\mathrm{OMN_p}$ as $R_{\mathrm{opt\_p}}$ and set the reference impedance of port 2 of $\mathrm{OMN_p}$ as $(1+1/\delta)Z_{\mathrm{L}}$. The expression of the scattering coefficient matrix is shown in Eq. (9).

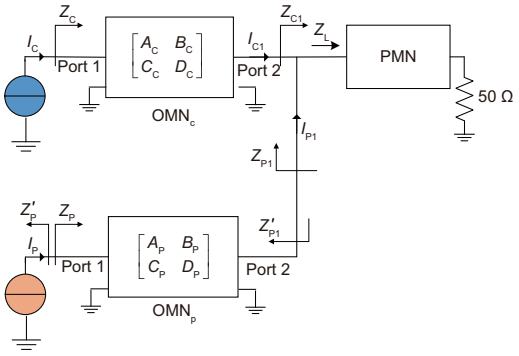

Fig. 1 Topology of the simplified traditional Doherty power amplifier

$$\begin{bmatrix} S_{11_{\mathrm{C}}} & S_{12_{\mathrm{C}}} \\ S_{21_{\mathrm{C}}} & S_{22_{\mathrm{C}}} \end{bmatrix} = \begin{bmatrix} 0 & \mathrm{e}^{\mathrm{j}\theta_{\mathrm{C}}} \\ \mathrm{e}^{\mathrm{j}\theta_{\mathrm{C}}} & 0 \end{bmatrix}. \tag{8}$$

$$\begin{bmatrix} S_{11_{\mathrm{P}}} & S_{12_{\mathrm{P}}} \\ S_{21_{\mathrm{P}}} & S_{22_{\mathrm{P}}} \end{bmatrix} = \begin{bmatrix} 0 & \mathrm{e}^{\mathrm{j}\theta_{\mathrm{P}}} \\ \mathrm{e}^{\mathrm{j}\theta_{\mathrm{P}}} & 0 \end{bmatrix}. \tag{9}$$

Hence, according to Frickey (1994), the ABCD matrix of $\mathrm{OMN_c}$ can be calculated. The specific expression of $\mathrm{OMN_c}$ is shown in Eq. (10):

$$\begin{cases} A_{\mathrm{C}} = \dfrac{R_{\mathrm{opt\_c}}(1+\mathrm{e}^{\mathrm{j}2\theta_{\mathrm{C}}})}{2\mathrm{e}^{\mathrm{j}2\theta_{\mathrm{C}}}\sqrt{R_{\mathrm{opt\_c}}Z_{\mathrm{L}}}}, \\ B_{\mathrm{C}} = \dfrac{R_{\mathrm{opt\_c}}(R_{\mathrm{opt\_c}} - \mathrm{e}^{\mathrm{j}2\theta_{\mathrm{C}}}Z_{\mathrm{L}})}{2\mathrm{e}^{\mathrm{j}2\theta_{\mathrm{C}}}\sqrt{R_{\mathrm{opt\_c}}Z_{\mathrm{L}}}}, \\ C_{\mathrm{C}} = \dfrac{1-\mathrm{e}^{\mathrm{j}2\theta_{\mathrm{C}}}}{2\mathrm{e}^{\mathrm{j}2\theta_{\mathrm{C}}}\sqrt{R_{\mathrm{opt\_c}}Z_{\mathrm{L}}}}, \\ D_{\mathrm{C}} = \dfrac{R_{\mathrm{opt\_c}} + \mathrm{e}^{\mathrm{j}2\theta_{\mathrm{C}}}Z_{\mathrm{L}}}{2\mathrm{e}^{\mathrm{j}2\theta_{\mathrm{C}}}\sqrt{R_{\mathrm{opt\_c}}Z_{\mathrm{L}}}}. \end{cases} \tag{10}$$

Similarly, the ABCD matrix of $\mathrm{OMN_p}$ can be calculated, and the specific expression is expressed as

$$\begin{cases} A_{\mathrm{P}} = \dfrac{R_{\mathrm{opt\_p}}(1+\mathrm{e}^{\mathrm{j}2\theta_{\mathrm{P}}})}{2\mathrm{e}^{\mathrm{j}2\theta_{\mathrm{P}}}\sqrt{R_{\mathrm{opt\_p}}Z_{\mathrm{L}}}}, \\ B_{\mathrm{P}} = \dfrac{R_{\mathrm{opt\_p}}(R_{\mathrm{opt\_p}} - \mathrm{e}^{\mathrm{j}2\theta_{\mathrm{P}}}Z_{\mathrm{L}})}{2\mathrm{e}^{\mathrm{j}2\theta_{\mathrm{P}}}\sqrt{R_{\mathrm{opt\_p}}Z_{\mathrm{L}}}}, \\ C_{\mathrm{P}} = \dfrac{1-\mathrm{e}^{\mathrm{j}2\theta_{\mathrm{P}}}}{2\mathrm{e}^{\mathrm{j}2\theta_{\mathrm{P}}}\sqrt{R_{\mathrm{opt\_p}}Z_{\mathrm{L}}}}, \\ D_{\mathrm{P}} = \dfrac{R_{\mathrm{opt\_p}} + \mathrm{e}^{\mathrm{j}2\theta_{\mathrm{P}}}Z_{\mathrm{L}}}{2\mathrm{e}^{\mathrm{j}2\theta_{\mathrm{P}}}\sqrt{R_{\mathrm{opt\_p}}Z_{\mathrm{L}}}}. \end{cases} \tag{11}$$

2.2.2 Calculating Z_{C1} at OBO

When DPA works at OBO, the impedance Z'_{P1B} in Fig. 2a (the impedance looking into OMN_p at the combining point) is not infinite and can be considered as a passive impedance (Shi et al., 2017). Therefore, $Z_{C1B} = Z'_{P1B}||Z_L$, and Z'_{P1B} is Z'_{P1} at OBO. Subsequently, analyze the specific value of Z'_{P1B}. Based on the nature of the reciprocal networks, we have $AD - BC = 1$ and Eq. (7), and the impedance expression of Z'_{P1} can be derived as shown in Eq. (12). When the peaking PA is not turned on, Z'_P can be regarded as infinite and the expression of Z'_{P1B} which is the impedance of Z'_{P1} at the OBO is shown in Eq. (13). The expression of Z_{C1B} is shown in Eq. (14).

$$Z'_{P1} = \frac{D_P Z'_P + B_P}{C_P Z'_P + A_P}. \tag{12}$$

$$Z'_{P1B} = \frac{D_P}{C_P}. \tag{13}$$

$$Z_{C1B} = Z'_{P1B}||Z_L = \frac{Z_L D_P}{Z_L C_P + D_P}. \tag{14}$$

By substituting Eq. (14) into Eq. (7), the value of Z_{CB} is related to the coefficient of the ABCD matrix of OMN_c and OMN_p, as shown in Eq. (15). According to Eqs. (10) and (11), it can be derived that Z_{CB} is determined by the phase characteristics θ_C of OMN_c and θ_P of OMN_p.

$$Z_{CB} = \frac{A_C D_P Z_L + B_C(Z_L C_P + D_P)}{C_C D_P Z_L + D_C(Z_L C_P + D_P)}. \tag{15}$$

Set Z_L as a complex value: $Z_L = R_L + jX_L$. The real part of Z_L is a fixed value: $R_L = R_{opt\_c}/(\delta + 1)$. Given a wide range to the imaginary part X_L of the complex impedance Z_L, hence a free parameter X_L will be obtained to extend the high-efficiency range of the designed DPA. Then, set the range of θ_C and θ_P: $\theta_C \in (-360°, 0°)$, $\theta_P \in (-360°, 0°)$. It can be concluded that the impedance Z_{CB} has three variables, namely, the phase parameter θ_C of OMN_c, θ_P of OMN_p, and the input impedance Z_L of PMN. Therefore, Z_{CB} is a function determined by these three variables, that is, $Z_{CB} = f(\theta_C, \theta_P, Z_L)$.

To make the designed DPA achieve high efficiency at the OBO across a wide frequency band, Z_{CB} should meet the continuous class-J mode (Shi et al., 2018). Fig. 3a gives the fundamental parameter space of the continuous class-J mode (the blue point locus). The fundamental impedance space of the continuous class-J mode is represented in Eq. (16) (Wright et al., 2009). According to Section 2.1, R_{opt_c}, R_{opt_p}, and δ are all known, and then, substitute them into $f(\theta_C, \theta_P, Z_L)$.

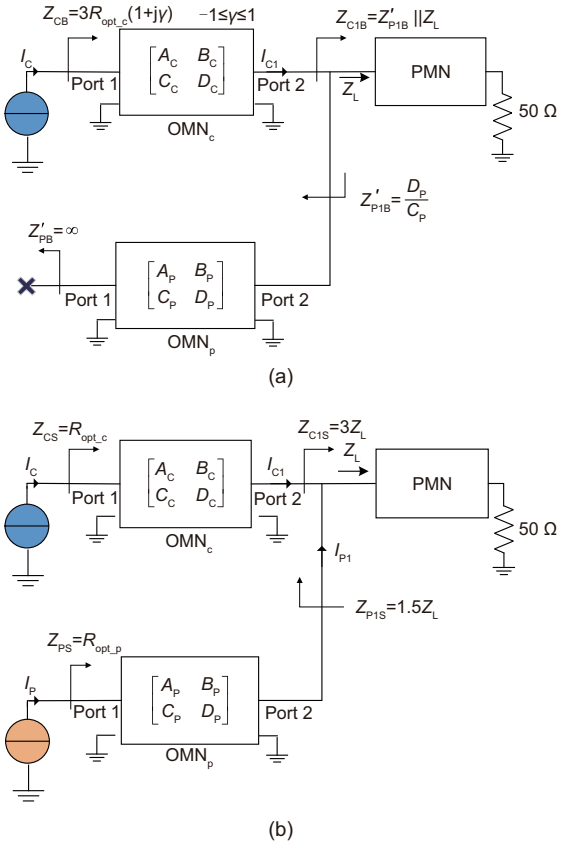

Fig. 2 Output matching network at output power back-off (a) and saturation (b)

$$Z_{J1} = (1 + \delta)(1 + j\gamma)R_{opt\_c}, \quad -1 \le \gamma \le 1. \tag{16}$$

To find the parameter solution space that makes Z_{CB} meet the continuous class-J mode in Eq. (16), a screening method is proposed in Eq. (17). If the difference between the real part of the calculated Z_{CB} and 48 ($3R_{opt\_c}$) is less than or equal to 0.8 ($0.05R_{opt\_c}$), and the imaginary part is between $-3R_{opt\_c}$ and $3R_{opt\_c}$, this set of variables $[\theta_C, \theta_P, Z_L]$ can be regarded as a subset of the high-efficiency solution space, as shown in Fig. 4. According to Section 2.2.1 and Eqs. (2)–(5), at saturation, OMN_c and OMN_p are in the matching state and the impedance Z_C and Z_P are R_{opt_c} and R_{opt_p}, respectively. Therefore, when PA operates in saturation, high efficiency can be achieved as shown in

Fig. 2b.

$$\begin{aligned}&\left|\mathrm{Re}\left\{f\left(\theta_{\mathrm{C}},\theta_{\mathrm{P}},Z_{\mathrm{L}}\right)-(\delta+1)R_{\mathrm{opt\_c}}\right\}\right|\le 0.05R_{\mathrm{opt\_c}},\\&\left|\mathrm{Img}\left\{f\left(\theta_{\mathrm{C}},\theta_{\mathrm{P}},Z_{\mathrm{L}}\right)\right\}\right|\le(\delta+1)R_{\mathrm{opt\_c}}.\end{aligned}\tag{17}$$

2.2.3 Using the solution set space $[\theta_{\mathrm{C}},\theta_{\mathrm{P}},Z_{\mathrm{L}}]$ to design the output network of DPA

The parameter solution space obtained is shown in Fig. 4. Through Section 2.2.2, the parameter solution space is the set of many groups of $[\theta_{\mathrm{C}},\theta_{\mathrm{P}},Z_{\mathrm{L}}]$. θ_{C}, θ_{P}, and Z_{L} of each group correspond one to one. Therefore, as long as one of the variables has been determined, another variable can be found.

According to the general method, θ_{C} and θ_{P} for the center frequency point are $-90°$ and $-180°$, respectively, which serve as the benchmark for selecting other parameter solutions to be assigned to other frequency points within the bandwidth. However, we avoid this approach because even if a DPA designed using this method achieves good performance, it cannot validate the correctness of the proposed method. It is quite likely that this good performance may be attributed to the traditional DPA theory. Therefore, it is necessary to select parameter solutions that are far from $[\theta_{\mathrm{C}},\theta_{\mathrm{P}}]=[-90°,-180°]$ to verify the correctness of the theory.

Since the absolute value of the phase characteristics of the passive network composed of microstrip lines will generally increase with the increase of frequency, θ_{C} and θ_{P} should increase with the increase of frequency. In addition, the range of variation of the imaginary part of Z_{L} with frequency should not be too large, so that it is not convenient for the design of PMN. The corresponding relationship between the selected parameter solutions and frequencies is shown in Table 1, indicating that the absolute values of θ_{C} and θ_{P} increase as the frequency increases. Fig. 5 illustrates the variation curves of θ_{C} and θ_{P} with respect to frequency. Next, $\mathrm{OMN_c}$ and $\mathrm{OMN_p}$ are designed. The variation of θ_{C}, θ_{P}, and Z_{L} with frequency should be consistent with that given in Table 1. At OBO, the fundamental impedance of Z_{C} is in the continuous class-J mode in Fig. 3a. Therefore, the designed DPA can achieve high efficiency at both saturation and OBO. The trajectories of Z_{C} and Z_{P} from OBO to saturation across the working frequency band are given in Fig. 3.

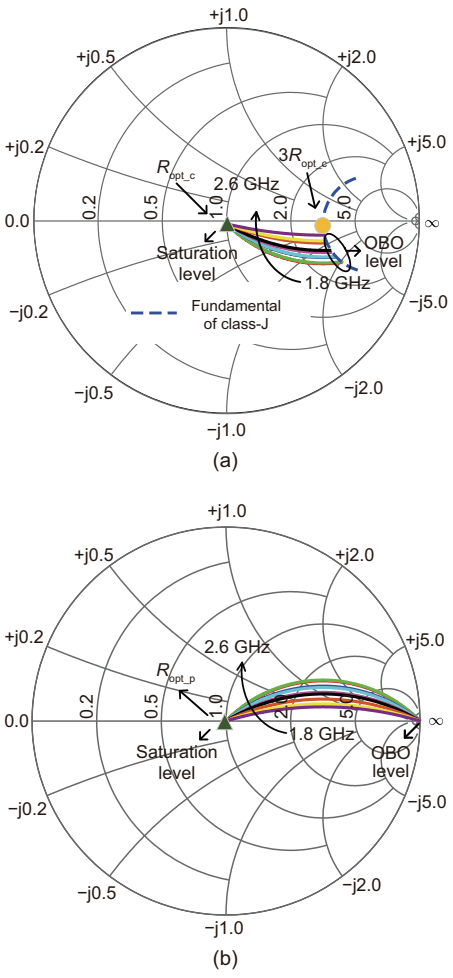

Fig. 3 Theoretical trajectories of Z_{C} (a) and Z_{P} (b) from the output power back-off (OBO) to the saturation level across the working frequency band. References to color refer to the online version of this figure

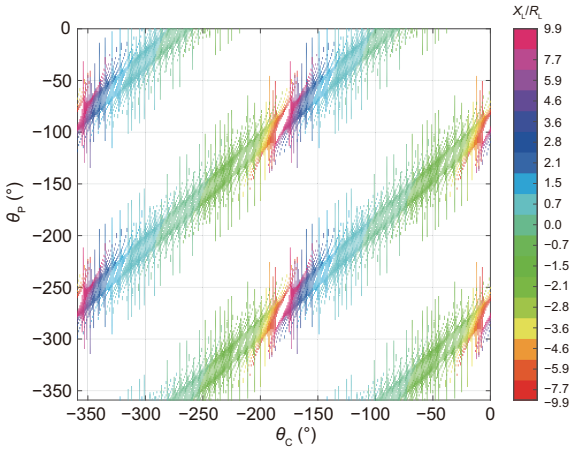

Fig. 4 The parameter solution space $[\theta_{\mathrm{C}},\theta_{\mathrm{P}},Z_{\mathrm{L}}]$

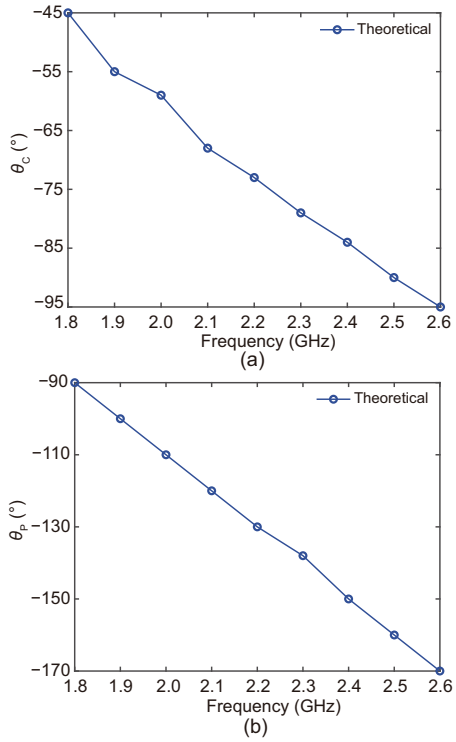

Fig. 5 Theoretical θ_C of OMN_c over the working frequency band (a) and theoretical θ_P of OMN_p over the working frequency band (b)

Table 1 Theoretical parameters at frequencies over 1.8–2.6 GHz

Frequency (GHz)	θ_C (°)	θ_P (°)	X_L/R_L
1.8	−45	−90	−1.00
1.9	−55	−100	−0.69
2.0	−59	−110	−0.60
2.1	−68	−120	−0.40
2.2	−73	−130	−0.31
2.3	−79	−138	−0.19
2.4	−84	−150	−0.10
2.5	−90	−160	0
2.6	−95	−170	0.10

$R_L = \frac{1}{3}R_{opt\_c}$

3 Design and simulation

In this section, based on the parameter solution space obtained in Section 2, an asymmetric DPA working over 1.8–2.6 GHz is designed. The CGH40025F transistor is selected for carrier PA, whereas the CGH40045F transistor is used for peaking PA. The maximum current ratio of the peaking PA to the carrier PA is equal to 2. Therefore, 9.5 dB OBO level can be achieved. The circuit is implemented on the substrate of Rogers 4350B with a thickness of H=0.508 mm and $\varepsilon = 3.66$. The drain bias voltages of the two transistors are both set to 28 V. The whole DPA consists of the power divider circuit, input matching network circuit, output matching circuits, and PMN.

The output matching circuits consist of OMN_c and OMN_p. Owning to the parasitic effect and packaging elements in the transistor, the packaged elements should be incorporated into OMN_c and OMN_p. The following goals should be met in the design: (1) when the DPA is in the saturated state, OMN_c and OMN_p achieve the matching state as shown in Fig. 2b; (2) The phase characteristics of OMN_c and OMN_p, (θ_C and θ_P), should be consistent with those in Table 1. Fig. 6 shows the designed circuit schematic OMN_c and OMN_p together with the packaged elements. Fig. 6 also shows the curves of θ_C and θ_P with frequency. Among them, the orange line is the phase parameter of Table 1 versus frequency and the blue line is the simulated phase parameter versus frequency. It can be concluded that the simulated results are basically the same as the theoretical results. After completing the design of OMN_c and OMN_p, PMN should be designed to match the 50 Ω antenna load to Z_L. PMN is designed based on the relationship between the input impedance Z_L and the frequency given in Table 1. The schematic of the PMN is shown in Fig. 7. The theoretical value of the input impedance is represented by a blue line, and the simulation value is represented by an orange line. Finally, the input matching circuit and the power divider are designed. The function of the input matching circuit is to transmit the signal to the transistor almost losslessly. The power divider adopts the three-stage Wilkinson asymmetric power dividers and the distribution power ratio of carrier PA to peaking PA is 4:7. The circuit structure of the power divider is shown in Fig. 8. Fig. 9 is the whole circuit diagram. To simplify the circuit structure, the circuit structure of the power divider is replaced by its geometry. To allow the output current of the carrier PA and the peaking PA maintain the same phase at the combining point at saturation, a phase compensation line is added between the power divider and the input matching circuit of the carrier PA. The simulated result of the designed DPA is shown in Fig. 10. The DPA achieves the drain efficiencies of 46.39%–54% and 49.2%–65% at 9.5 dB OBO and saturation, respectively. The maximum output power of the designed DPA is 47.2–48.7 dBm with a saturation gain of 6–7 dB over the whole working frequency band.

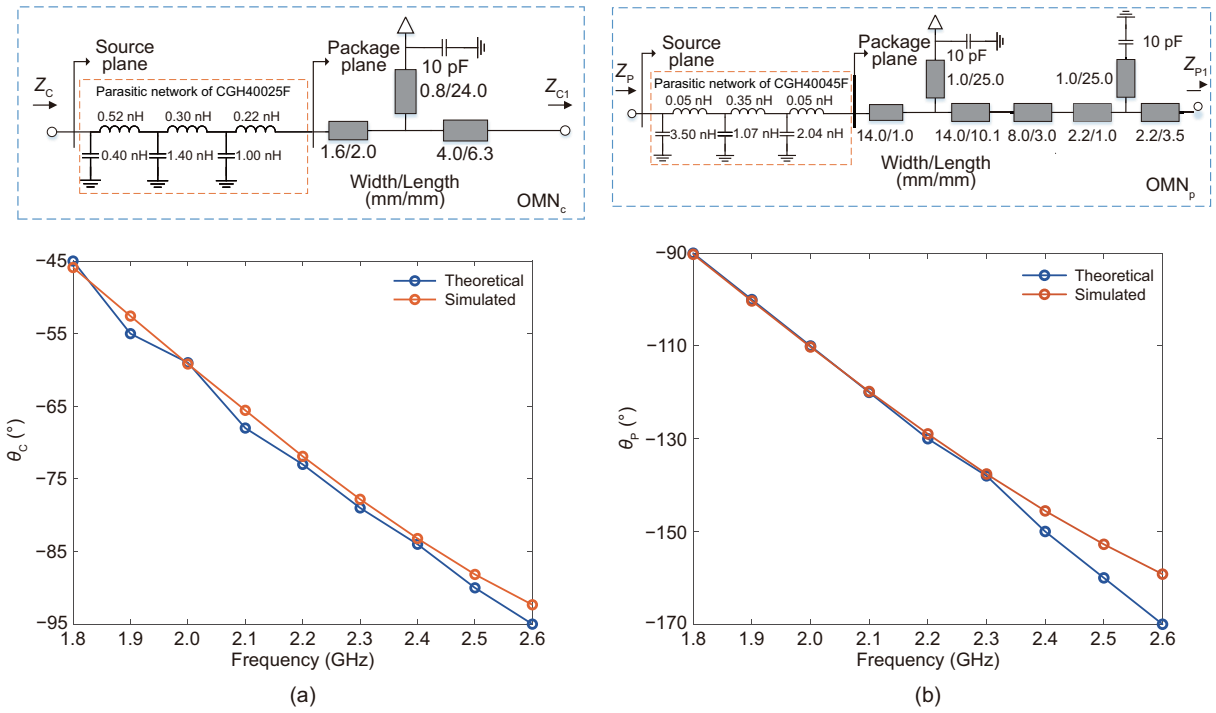

Fig. 6 Schematic (top) and phase parameter (bottom) of the output matching network: (a) OMN_c; (b) OMN_p. References to color refer to the online version of this figure

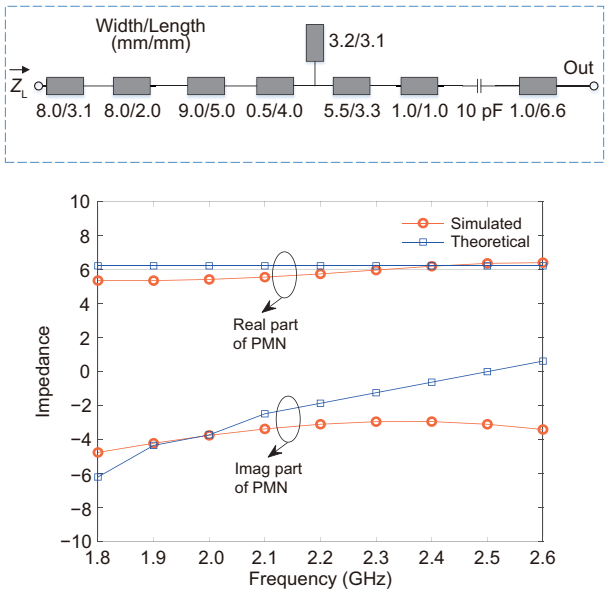

Fig. 7 Schematic of the post-matching network (top) and its input impedance across the working frequency band (bottom). References to color refer to the online version of this figure

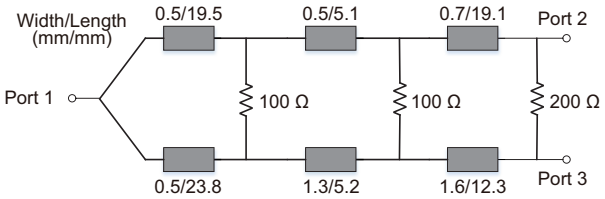

Fig. 8 Schematic of the designed three-stage Wilkinson power divider

4 Experimental results

The fabricated DPA is shown in Fig. 11. The size of the fabricated DPA is 110 mm × 70 mm. To test the performance of the fabricated DPA, drain efficiency (DE), gain, and adjacent channel power ratio (ACPR) of the designed DPA are tested using the continuous wave and modulated signal.

4.1 Small-signal measurements

The performance of the fabricated DPA is assessed using a vector network analyzer. Fig. 12 shows the measured S-parameters from 1.8 to 2.6 GHz, alongside the simulated data for comparison. For S_{21}, the measured results closely match the simulated ones, both showing lower gain at higher frequencies. However, there are discrepancies between the measured and simulated S_{21} values, likely due to limitations in the accuracy of the simulation model used in the advanced design system (ADS).

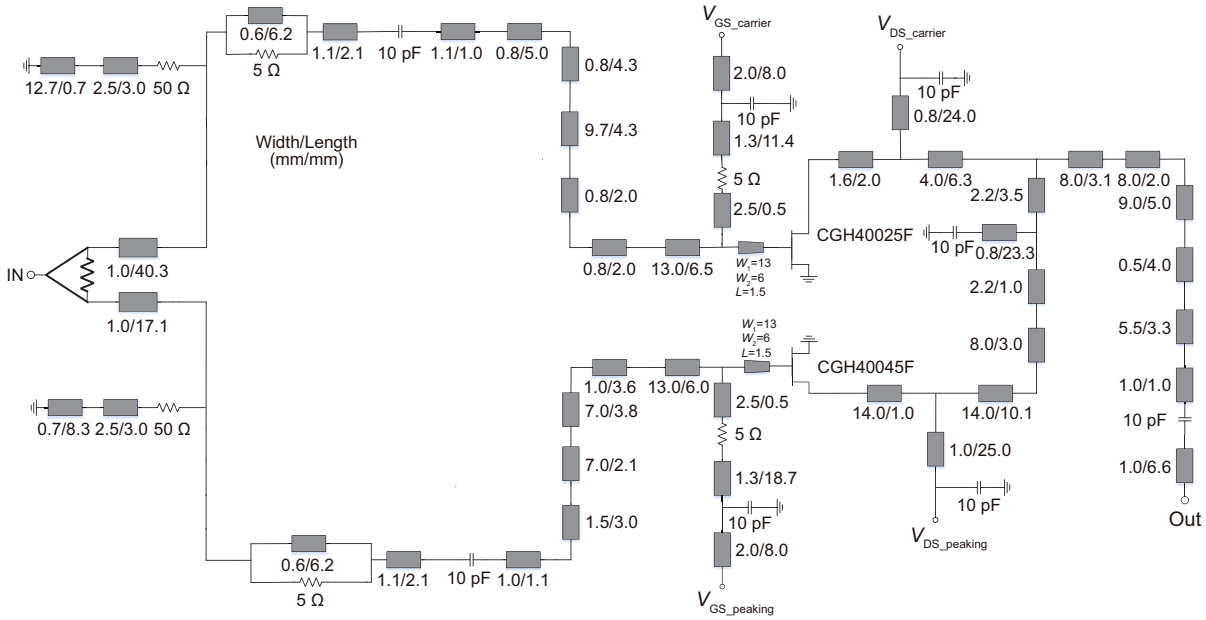

Fig. 9 Schematic of the proposed Doherty power amplifier

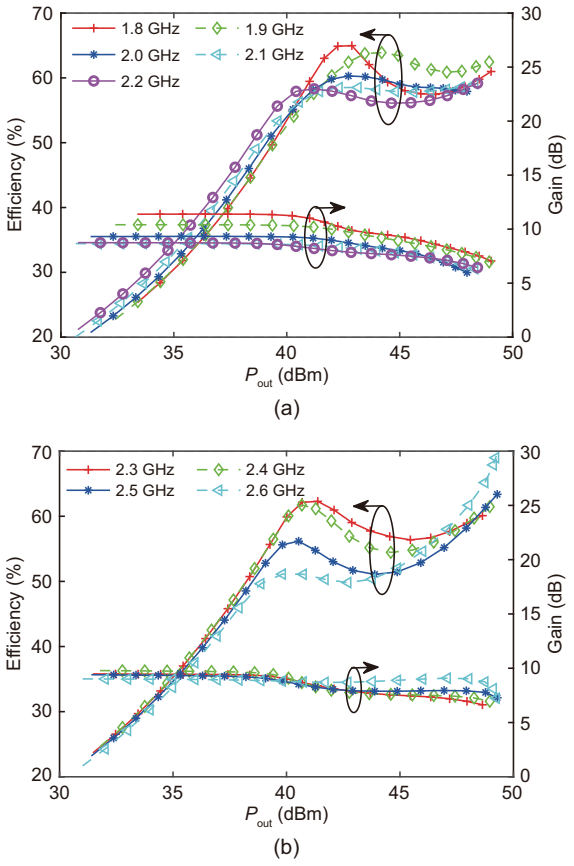

Fig. 10 Simulated drain efficiencies and gains of the designed Doherty power amplifier over output power: (a) 1.8–2.2 GHz; (b) 2.3–2.6 GHz

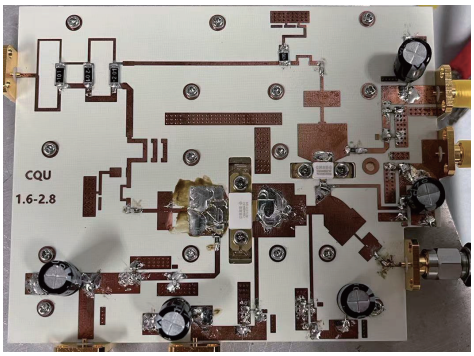

Fig. 11 Photograph of the fabricated Doherty power amplifier

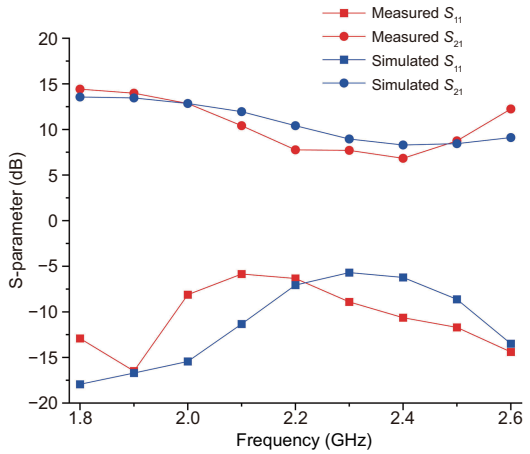

Fig. 12 Simulated and measured S-parameters of the Doherty power amplifier

4.2 Continuous wave singal measurements

DE and gain of the fabricated DPA are measured using continuous wave signals across 1.8–2.6 GHz with 100 MHz frequency step. Fig. 13 depicts the measurement setup adopted. A vector signal generator (VSG) is responsible for generating the input signal. This signal is then channeled through a driver and an isolator before being fed into the design under the test (DUT). The output signal from the DPA passes through an attenuator, and ultimately, the measurement results are visualized on a vector spectrum analyzer. When the signal operates in the frequency range of 1.8–2.0 GHz, the gate bias of the peaking PA is set to –7.5 V. When the signal operates in the frequency range of 2.1–2.6 GHz, the gate bias of the peaking PA is set to –8.1 V. The drain voltages of both amplifiers are set to 28 V.

The measured DE and gain are shown in Fig. 14. According to Fig. 14, the DPA can achieve the saturated DE of 45.8%–71.1% with an output power of 46.9–48.8 dBm. At the 9.5 dB OBO level, 42.7%–56.4% DE is achieved. The gain at the saturation power is 5.5–8.0 dB. The power-added efficiency (PAE) of this fabricated DPA is shown in Fig. 15. DPA can achieve saturated PAE of 36.6%–49.7%. At the 9.5 dB OBO level, 26.5%–50.4% PAE is achieved. At high frequencies, the lower gain of the DPA may be caused by mismatch issues between the power divider and the input matching circuit. By comparing Figs. 10 and 14, it can be found that at low frequencies, there is a certain difference between the simulated efficiency and the measured efficiency. Analyzing the reason, it may be that there is a certain error between the transistor model used by the ADS simulation platform and the actual transistor. Moreover, the nonlinear capacitance of the transistor has a certain effect on the phase in the actual measurement, which results in the current phase difference at the combining point not being 0, which causes the mismatch of the output matching network and affects the efficiency. In addition, the temperature has an effect on the measured results.

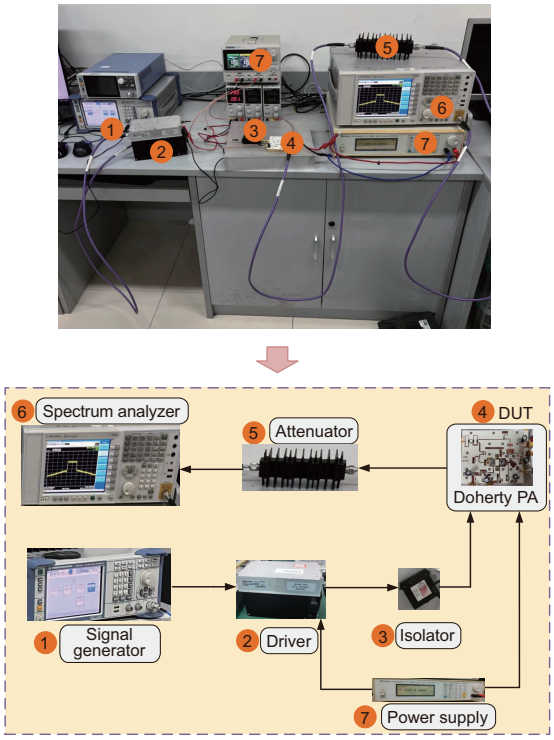

Fig. 13 Large-signal CW signal measurement setup

4.3 Long-term evolution (LTE) modulated-signal measurements

The high-linearity PA can enhance the quality of communication services. Nonlinear distortion will

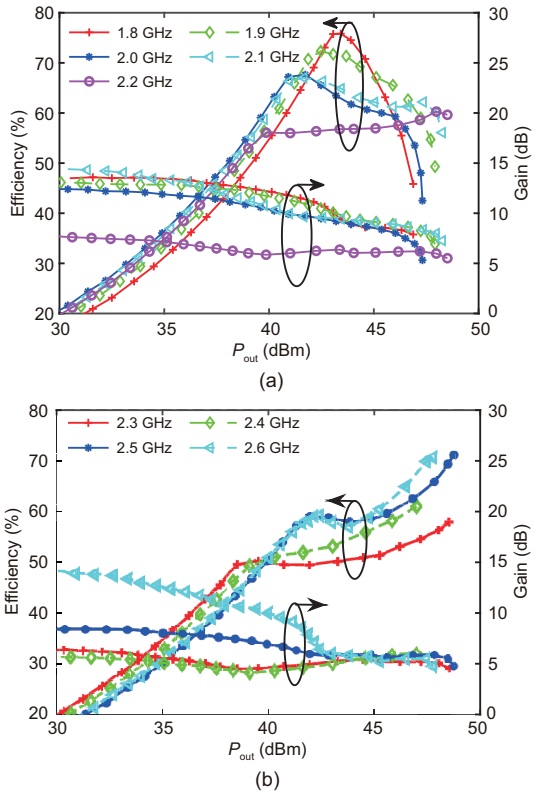

Fig. 14 Measured drain efficiencies and gains of the designed Doherty power amplifier over output power: (a) 1.8–2.2 GHz; (b) 2.3–2.6 GHz

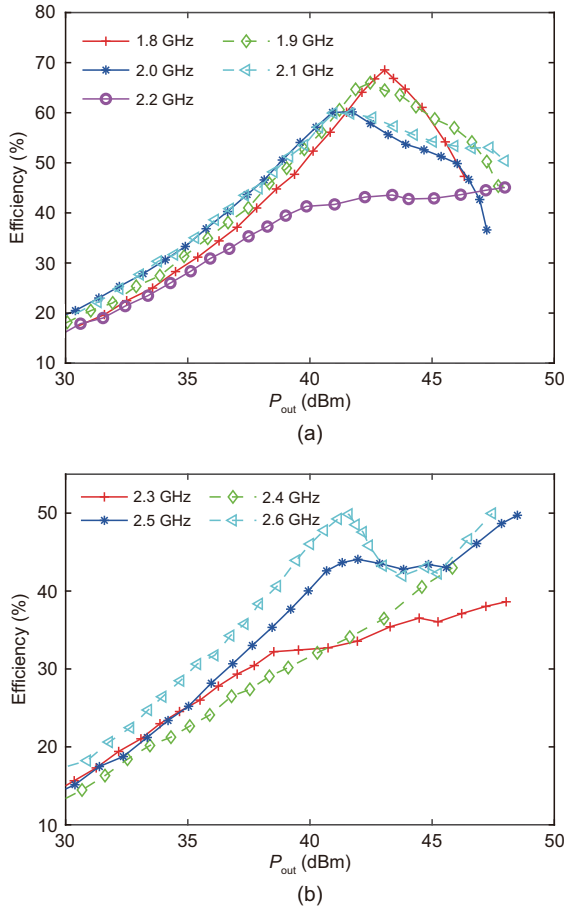

Fig. 15 Measured power-added efficiencies of the designed Doherty power amplifier over output power: (a) 1.8–2.2 GHz; (b) 2.3–2.6 GHz

lead to system error, out-of-band radiation, and interference with other channels, which seriously affects the quality and reliability of the communication system (Cui et al., 2023). To evaluate the linearity of the fabricated DPA, a long-term evolution (LTE) signal with a PAPR of 8 dB and a signal bandwidth of 20 MHz is used. Fig. 16 shows the measured DE, average output power, and ACPR across the entire 1.8–2.6 GHz band. The DPA achieves an average DE of 42.1%–55.5% and ACPR between −23.8 dBc and −35.5 dBc in the operation band. An average output power of 38–39.4 dBm is also observed. The normalized power spectra of the fabricated DPA at 1.8, 2.1, and 2.6 GHz with or without digital pre-distortion (DPD) are displayed in Fig. 17, all of which have been gridded. The output power is 38.1, 36.8, and 39 dBm with a DE of 54.3%, 55.5%, and 51.6%, respectively. As shown in Fig. 17, better than 49 dBc ACPR is obtained after DPD and more than 20 dB improvement is achieved compared to the original

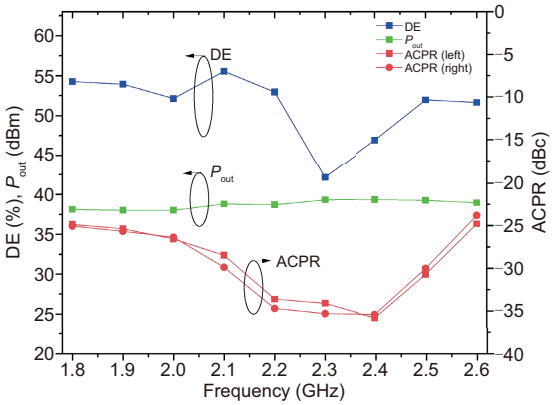

Fig. 16 Measured average drain efficiency (DE), average output power, and adjacent channel power ratio (ACPR) versus frequency

ACPR of PA output signals. Fig. 18 shows the setup for DPD performance measurement.

The error vector magnitude (EVM) of −10.2, −12, and −11.4 dB is achieved at 1.8, 2.1, and 2.6 GHz, respectively. After the DPD performed, the EVM can be improved to −37.7, −37.1, and −42 dB, respectively, at these three frequencies. The DPD algorithm used is a generalized memory polynomial (GMP) model under a direct learning structure (closed loop) with 10 iterations for the coefficient solution. It has the nonlinearity order Ka=[0: 11], memory depth La = [0: 4], nonlinearity of the lagged cross-term order Kb=[0: 7], memory depth of the lagged cross-term Lb=[0: 4], lagged cross-depth Mb=[0: 2], model coefficient of the leading cross terms Kc=[0: 5], and memory depth of leading cross terms Lc=[0: 3].

Measured performance is compared to that of the previously reported DPAs with an extended back-off range as given in Table 2. Compared with most of the works in Table 2, the proposed DPA shows better broadband performance and efficiency index, with a relative bandwidth of 36.4%. Besides, this kind of DPA design incorporates transistors with higher saturation power, enabling a significantly higher output power. Additionally, due to the larger size of the transistors used in this design, their parasitic parameters are increased and the optimal impedance shows a stronger degree of discreteness, posing considerable challenges in the design process. The DPA designed using the parameter solution space method proposed in this paper has yielded relatively impressive results. This achievement not only validates the correctness of the

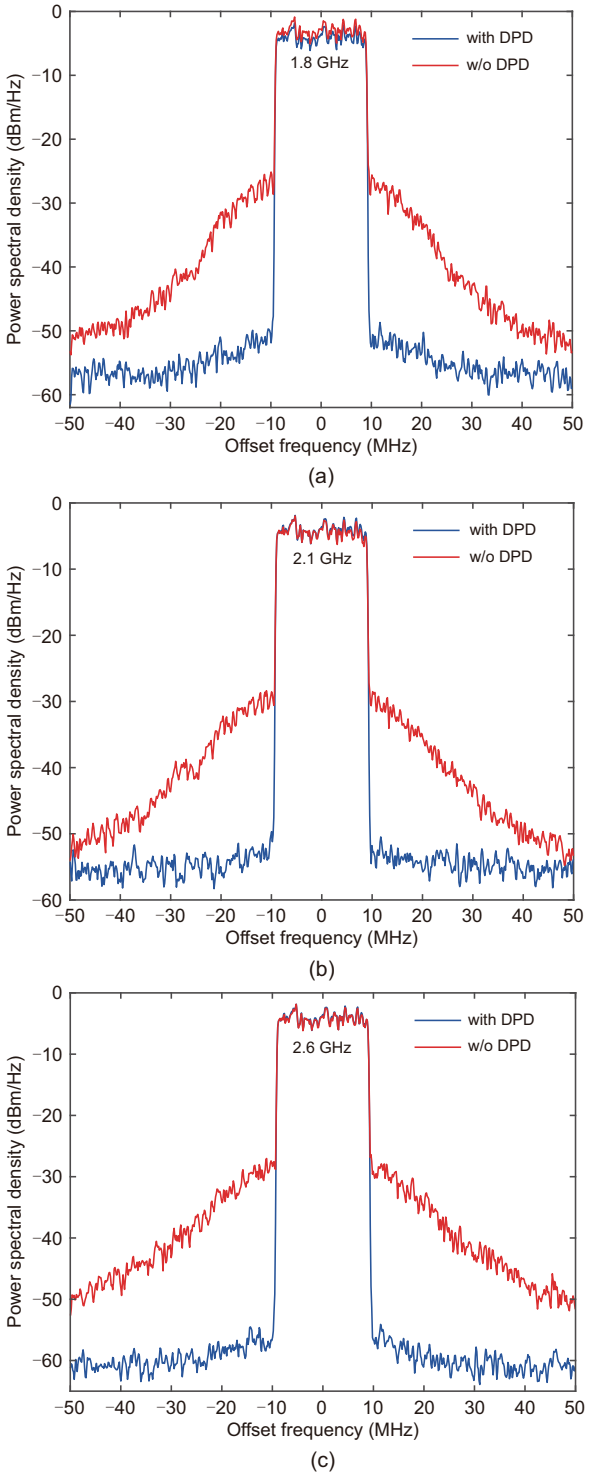

Fig. 17 Measured normalized power spectral density using 20 MHz long-term evolution signals with peak-to-average power ratio equal to 8 dB: (a) 1.8 GHz; (b) 2.1 GHz; (c) 2.6 GHz (DPD: digital pre-distortion; w/o: without)

proposed parameter solution space but also demonstrates its effectiveness in practical design.

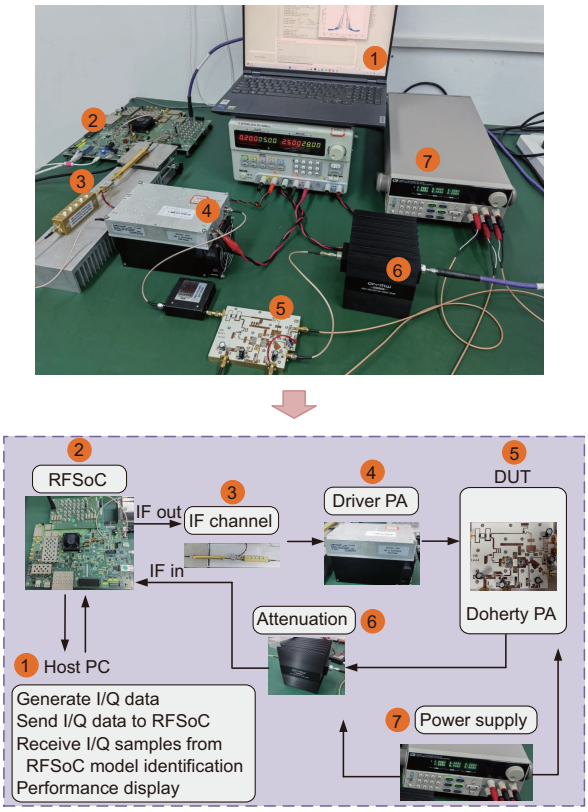

Fig. 18 Setup for digital pre-distortion (DPD) performance measurement

5 Conclusions

In this paper, the input impedance of the PMN is set to a complex value and the solution set $[\theta_C, \theta_P, Z_L]$ that makes the DPA achieve high efficiency at the OBO is obtained according to the basic principle of the DPA. Based on this solution set, an asymmetric DPA working over 1.8–2.6 GHz is constructed. The DPA can achieve an efficiency of 42.7%–56.4% and 45.8%–71.1% at the 9.5 dB OBO level and saturation level, respectively. The saturation output power is 46.9–48.8 dBm with a saturated gain of 5.5–8.0 dB.

Contributors

Cheng BI, Zhijiang DAI, and Jingzhou PANG designed the research. Cheng BI drafted the paper. Haotian LI, Shuai WANG, Kang ZHONG, Jingsong WANG, and Ruibin GAO helped organize the paper. Zhijiang DAI revised and finalized the paper.

Conflict of interest

All the authors declare that they have no conflict of interest.

Table 2 Performance comparison

Reference	Technique	Topology	Frequency (GHz)	FBW (%)	Power (dBm)	OBO (dB)	DE@OBO (%)	DE@SAT (%)	PAE@SAT (%)	ACPR (dBc)
Choi et al. (2021)	Smith chart	Asy.	1.68	–	43.5	9.5	54.7	56.4	53.6	–27.3 (1.68 GHz)
Li M et al. (2022)	Phase compensation	Asy.	1.55–2.2	35	45.2–47.3	11.1–13.2	42.2–52.1	47–62.7	33.1–51	–29.1 (2 GHz)
Zhou et al. (2022)	Phase compensation	Sym.	1.6–1.95	19.7	42.7–43.5	9–9.5	62.5–67.5	64.6–70.9	56.5–62.9	<–22
Li C et al. (2020)	Phase compensation	Sym.	1.9–2.4	23.3	44.2–49.7	8.5–9	44.2–49.7	65.2–71.8	52.8–56	–31.1 (2.4 GHz)
Xu et al. (2021)	Modified LMN	Asy.	1.4–2.5	56.4	44–45.9	9	44.6–54.6	61–75.5	53.2–66	–29.8 (1.6 GHz)
This work	Parameter solution space	Asy.	1.8–2.6	36.4	46.9–48.8	9.5	42.7–56.4	45.8–71.1	36.6–49.7	–33.6 (2.5 GHz)

ACPR: adjacent channel power ratio; Asy.: asymmetrical; DE: drain efficiency; FBW: fractional bandwidth; LMN: load modulation network; OBO: output power back-off; PAE: power-added efficiency; Power: saturation output power; Sym.: symmetrical; SAT: saturaion state

Data availability

The data that support the findings of this study are available from the corresponding author upon reasonable request.

References

Bachi J, Serhan A, Pham DKG, et al., 2022. A novel approach for Doherty PA design using a compact L-C combiner. *IEEE Trans Circ Syst II Express Briefs*, 69(10):4023-4027. https://doi.org/10.1109/TCSII.2022.3185174

Cavarroc M, Lamy A, Lembeye O, et al., 2023. Compact 40% fractional bandwidth Doherty PA with input group delay engineering. *IEEE Microw Wirel Technol Lett*, 33(6):851-854. https://doi.org/10.1109/LMWT.2023.3266095

Chen WJ, Wu YL, Li SB, et al., 2023. Fully-integrated broadband GaAs MMIC load modulated balanced amplifier for sub-6 GHz applications. *IEEE Trans Circ Syst II Express Briefs*, 70(8):2834-2838. https://doi.org/10.1109/TCSII.2023.3246042

Choi W, Kang H, Oh H, et al., 2021. Doherty power amplifier based on asymmetric cells with complex combining load. *IEEE Trans Microw Theory Tech*, 69(4):2336-2344. https://doi.org/10.1109/TMTT.2021.3059666

Cui J, Li PP, Sheng WX, 2023. High linearity U-band power amplifier design: a novel intermodulation point analysis method. *Front Inform Technol Electron Eng*, 24(1):176-186. https://doi.org/10.1631/FITEE.2200082

Doherty WH, 1936. A new high efficiency power amplifier for modulated waves. *Proc Inst Radio Eng*, 24(9):1163-1182. https://doi.org/10.1109/JRPROC.1936.228468

Fang XH, Cheng KKM, 2014. Extension of high-efficiency range of Doherty amplifier by using complex combining load. *IEEE Trans Microw Theory Tech*, 62(9):2038-2047. https://doi.org/10.1109/TMTT.2014.2333713

Frickey DA, 1994. Conversions between S, Z, Y, H, ABCD, and T parameters which are valid for complex source and load impedances. *IEEE Trans Microw Theory Tech*, 42(2):205-211. https://doi.org/10.1109/22.275248

Hallberg W, Özen M, Gustafsson D, et al., 2016. A Doherty power amplifier design method for improved efficiency and linearity. *IEEE Trans Microw Theory Tech*, 64(12):4491-4504. https://doi.org/10.1109/TMTT.2016.2617882

Li C, You F, Peng J, et al., 2020. Co-design of matching sub-networks to realize broadband symmetrical Doherty with configurable back-off region. *IEEE Trans Circ Syst II Express Briefs*, 67(10):1730-1734. https://doi.org/10.1109/TCSII.2019.2946395

Li M, Pang JZ, Li Y, et al., 2019. Ultra-wideband dual-mode Doherty power amplifier using reciprocal gate bias for 5G applications. *IEEE Trans Microw Theory Tech*, 67(10):4246-4259. https://doi.org/10.1109/TMTT.2019.2932977

Li M, Li ZQ, Zheng Q, et al., 2022. A 17–26.5 GHz 42.5 dBm broadband and highly efficient gallium nitride power amplifier design. *Front Inform Technol Electron Eng*, 23(2):346-350. https://doi.org/10.1631/FITEE.2000513

Li MY, Cheng XB, Dai ZJ, et al., 2023. A novel method for extending the output power back-off range of an asymmetrical Doherty power amplifier. *Front Inform Technol Electron Eng*, 24(3):470-479. https://doi.org/10.1631/FITEE.2200250

Li SS, Huang MY, Jung D, et al., 2021. A mm-wave current-mode inverse outphasing transmitter front-end: a circuit duality of conventional voltage-mode outphasing. *IEEE J Sol-State Circ*, 56(6):1732-1744. https://doi.org/10.1109/JSSC.2020.3038882

Pang JZ, He SB, Dai ZJ, et al., 2016. Design of a post-matching asymmetric Doherty power amplifier for broadband applications. *IEEE Microw Wirel Compon Lett*, 26(1):52-54. https://doi.org/10.1109/LMWC.2015.2505651

Rouhani S, Ghanaatian A, Abrishamifar A, et al., 2020. A wideband quasi-asymmetric Doherty power amplifier with a two-section matching-phase difference compensator network design using GaAs technology. *Analog Integr Circ Signal Process*, 105(3):359-370. https://doi.org/10.1007/s10470-020-01731-9

Shi WM, He SB, You F, et al., 2017. The influence of the output impedances of peaking power amplifier on

broadband Doherty amplifiers. *IEEE Trans Microw Theory Tech*, 65(8):3002-3013. https://doi.org/10.1109/TMTT.2017.2673822

Shi WM, He SB, Zhu XY, et al., 2018. Broadband continuous-mode Doherty power amplifiers with noninfinity peaking impedance. *IEEE Trans Microw Theory Tech*, 66(2):1034-1046. https://doi.org/10.1109/TMTT.2017.2749224

Son J, Kim I, Moon J, et al., 2011. A highly efficient asymmetric Doherty power amplifier with a new output combining circuit. IEEE Int Conf on Microwaves, Communications, Antennas and Electronic Systems, p.1-4. https://doi.org/10.1109/COMCAS.2011.6105792

Wright P, Lees J, Benedikt J, et al., 2009. A methodology for realizing high efficiency class-J in a linear and broadband PA. *IEEE Trans Microw Theory Tech*, 57(12):3196-3204. https://doi.org/10.1109/TMTT.2009.2033295

Xu Y, Pang JZ, Wang XY, et al., 2021. Enhancing bandwidth and back-off range of Doherty power amplifier with modified load modulation network. *IEEE Trans Microw Theory Tech*, 69(4):2291-2303. https://doi.org/10.1109/TMTT.2021.3056402

Yang ZX, Yao Y, Li MY, et al., 2019. Bandwidth extension of Doherty power amplifier using complex combining load with noninfinity peaking impedance. *IEEE Trans Microw Theory Tech*, 67(2):765-777. https://doi.org/10.1109/TMTT.2018.2884415

Zhang JR, Zheng SY, Yang N, 2023. An efficient broadband symmetrical Doherty power amplifier with extended back-off range. *IEEE Trans Circ Syst II Express Briefs*, 70(4):1316-1320. https://doi.org/10.1109/TCSII.2022.3227045

Zhang XH, Li SS, Huang DQ, et al., 2023. A millimeter-wave three-way Doherty power amplifier for 5G NR OFDM. *IEEE J Sol-State Circ*, 58(5):1256-1270. https://doi.org/10.1109/JSSC.2023.3238766

Zhou XY, Chan WS, Sharma T, et al., 2022. A Doherty power amplifier with extended high-efficiency range using three-port harmonic injection network. *IEEE Trans Circ Syst I Regul Pap*, 69(7):2756-2766. https://doi.org/10.1109/TCSI.2022.3160382